

Dynamical Signatures of Chaos to Integrability Crossover in 2×2 Generalized Random Matrix Ensembles

Adway Kumar Das & Anandamohan Ghosh

Department of Physical Sciences, Indian Institute of Science Education and Research
Kolkata, Mohanpur, 741246 India

E-mail: akd19rs062@iiserkol.ac.in, anandamohan@iiserkol.ac.in

15 November 2023

Abstract. We introduce a two-parameter ensemble of generalized 2×2 real symmetric random matrices called the β -Rosenzweig-Porter ensemble (β -RPE), parameterized by β , a fictitious inverse temperature of the analogous Coulomb gas model, and γ , controlling the relative strength of disorder. β -RPE encompasses RPE from all of the Dyson's threefold symmetry classes: orthogonal, unitary and symplectic for $\beta = 1, 2, 4$. Firstly, we study the energy correlations by calculating the density and 2nd moment of the Nearest Neighbor Spacing (NNS) and robustly quantify the crossover among various degrees of level repulsions. Secondly, the dynamical properties are determined from an exact calculation of the temporal evolution of the fidelity enabling an identification of the characteristic Thouless and the equilibration timescales. The relative depth of the correlation hole in the average fidelity serves as a dynamical signature of the crossover from chaos to integrability and enables us to construct the phase diagram of β -RPE in the γ - β plane. Our results are in qualitative agreement with numerically computed fidelity for $N \gg 2$ matrix ensembles. Furthermore, we observe that for large N the 2nd moment of NNS and the relative depth of the correlation hole exhibit a second order phase transition at $\gamma = 2$.

Keywords: Rosenzweig-Porter Ensemble, β -ensemble, level spacing, fidelity

Submitted to: *J. Phys. A: Math. Gen.*

1. Introduction

Random matrix theory provides important insights into the dynamical aspects of a system by analyzing its spectral statistics. For example, an integrable system behaves as an insulator while producing uncorrelated eigenvalues and localized eigenstates as in the Poisson ensemble [1]. Contrarily, Wigner-Dyson ensembles (WDE) [2, 3] can replicate the energy spectra in completely chaotic systems [4, 5] while respective eigenstates are

ergodic [6] leading to a diffusive transport of any excitation in the system. In a closed quantum system, the energy correlations and the eigenstate localization properties govern the dynamical response of the system, e.g. the *fidelity* of an initially localized state [7, 8]. The time required for the system to equilibrate and the equilibrium value of the fidelity are indicative of the degree of chaos in the system [9]. Such dynamical signatures can be measured experimentally and can identify various quantum mechanical phases [10, 11, 12]. While the integrable and chaotic limits are well characterized, the evidence of intermediate statistics have generated considerable interest in the context of many-body localization transition [13, 14, 15, 16, 17]. This necessitates exploring dynamical signatures of random matrix ensembles beyond the WDE.

The WDE have two constraints: statistical independence of the matrix elements and canonical invariance [18]. We need to relax either or both of these constraints to capture the intermediate spectral properties found in the systems deviating from the conventional Boltzmann statistics [19, 20, 21, 22, 23, 24, 25]. A prominent random matrix model without canonical invariance is the Rosenzweig-Porter Ensemble (RPE). It was originally introduced to explain the atomic spectra of elements like Y, Zr, Nb, Pd [26]. Since RPE is essentially Poisson ensemble perturbed by WDE, the perturbation strength can be considered as a fictitious time and RPE can be cast as a Brownian ensemble [27, 28, 29, 30, 31]. Again RPE can be considered as a deformed ensemble [32, 33, 34, 35] where the symmetries present in an integrable system are broken. Apart from the obvious appeal as an interpolating random matrix ensemble, interestingly, RPE hosts three distinct phases: ergodic, non-ergodic extended phase having fractal eigenstates and a localized phase [36, 37, 38, 39]. Corresponding phase transitions have been explored experimentally in microwave resonators [40]. The localized and critical states at the Anderson transition point of RPE have the same statistical properties as those in the hierarchical lattices such as Bethe lattice or Random Regular Graph [36]. The Fock space of generic isolated quantum many-body systems has a hierarchical structure [41], hence Anderson localization in RPE can serve as a toy model for the many-body localization. Therefore, RPE has gained a lot of attention in recent times and has been extensively studied [36, 42, 43, 44, 45, 46, 47, 48].

In this work, we focus on the dynamical properties of the 2×2 RPE to identify the crossover from chaos to integrability. The simplicity of 2×2 matrices makes them amenable to exact analytical treatments while capturing the essence of large system sizes, $N \gg 2$ [49, 50]. For example, the Wigner's surmise obtained for 2×2 WDE are reasonable approximations of the density of level spacing for large N . Apart from their simplicity, 2-level systems are often encountered in various disciplines e.g. optics [51, 52, 53, 54], wave localization [55], PT symmetry [56, 57], exciton dynamics [58], quantum information processing [59], beam shifts in quantum optics [60, 61, 62]. The matrix elements of 2×2 RPE follow Gaussian distributions with mean 0 and the variances [36]

$$\langle H_{n,n}^2 \rangle = 1, \quad \langle |H_{n,m}|^2 \rangle = \frac{\beta}{2^{\gamma+1}}, \quad \gamma \in \mathbb{R}, \quad (1)$$

where γ parameterizes the disorder strength and β is the Dyson's index characterizing the symmetry class, e.g. $\beta = 1, 2, 4$ correspond to real, complex, quaternion matrices from the orthogonal, unitary, symplectic symmetry classes, respectively. For 2×2 matrices from all the three symmetry classes, we compute the spectral statistics and the fidelity of an initially localized state. The ensemble averaged fidelity after an initial quadratic decay jumps and relaxes to an equilibrium value, decreasing with the loss of integrability. The dip, occurring before and below the equilibrium value, is known as the *correlation hole*. The relative depth of the correlation hole is denoted by κ and is used to quantify the crossover from chaos to integrability which is similar to that inferred from the spectral statistics. We introduce a two-parameter (γ, β) model called the β -Rosenzweig-Porter ensemble (β -RPE) which reduces to β -ensemble [63] for $\gamma = 0$. We derive an analytical expression of the fidelity as a function of time for β -RPE unifying all the abovementioned symmetry classes. We numerically obtain a phase diagram of β -RPE using κ to identify the crossover from chaos to integrability in the γ - β plane. Based on the analytical expression of fidelity of 2×2 β -ensemble, we propose an ansatz for the average fidelity of any 2-level systems, therefore providing a dynamical counterpart of the empirical distributions of spectral statistics. We have numerically computed fidelity for $N \gg 2$ matrices and show that the relative depth of the correlation hole exhibit a second order phase transition at $\gamma = 2$ for RPE from all the three symmetry classes. In spite of the simplicity, the dynamical signatures of parameter dependent crossover in 2-level system possess qualitative similarity to those of random matrices with $N \gg 2$.

2. Orthogonal Rosenzweig-Porter Ensemble (O-RPE)

For a choice of orthogonal eigenvectors, $|\Phi_1\rangle = \begin{pmatrix} \cos \theta \\ -\sin \theta \end{pmatrix}$ and $|\Phi_2\rangle = \begin{pmatrix} \sin \theta \\ \cos \theta \end{pmatrix}$ with the eigenvalues E_1 and E_2 , respectively, any 2×2 real symmetric matrix can be expressed as

$$H = \begin{pmatrix} E_1 \cos^2 \theta + E_2 \sin^2 \theta & \frac{1}{2}(E_1 - E_2) \sin 2\theta \\ \frac{1}{2}(E_1 - E_2) \sin 2\theta & E_1 \sin^2 \theta + E_2 \cos^2 \theta \end{pmatrix}. \quad (2)$$

The Jacobian of the transformation from matrix space to eigenspace is the Vandermonde determinant, $E_1 - E_2$. Then following equation 1, we obtain the joint density of eigenvalues and θ for 2×2 O-RPE as

$$P(E_1, E_2, \theta) = \frac{2^{\frac{\gamma}{2}}}{4\pi^{\frac{3}{2}}} |E_1 - E_2| e^{-\frac{E_1^2 + E_2^2}{2} + (1-2\gamma) \sin^2 2\theta \frac{(E_1 - E_2)^2}{4}}. \quad (3)$$

The energy correlation can be captured by the Nearest Neighbor Spacing (NNS), $S = |E_1 - E_2|$ [64] and the corresponding density is given by

$$P(S) = \int_0^\pi d\theta P(S, \theta) = \int_0^\pi d\theta \int_{-\infty}^\infty dE_1 dE_2 P(E_1, E_2, \theta) \delta(S - |E_1 - E_2|). \quad (4)$$

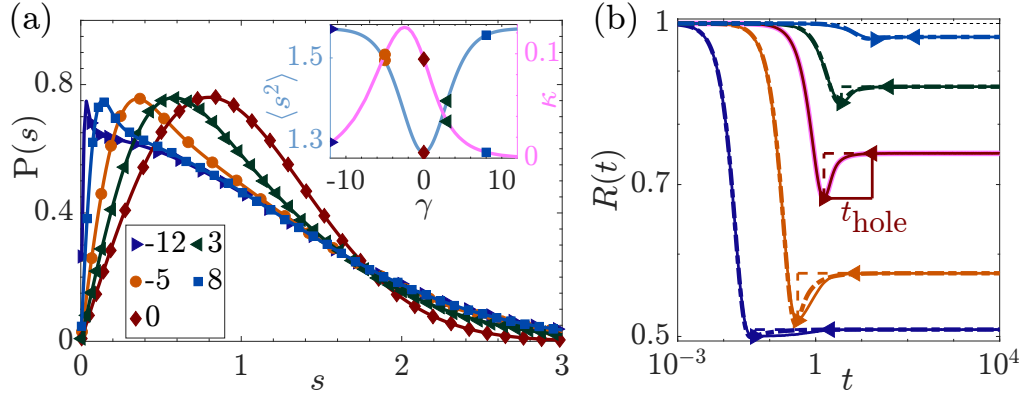


Figure 1. O-RPE: (a) density of NNS for various γ . Solid lines denote analytical form in equation 5 whereas the markers denote simulation over 10^7 samples. Inset shows $\langle s^2 \rangle$, 2nd moment of NNS, where the blue solid line denotes analytical form in table 1 and κ , the relative depth of the correlation hole in the fidelity (pink solid line). (b) temporal evolution of fidelity where Thouless and relaxation times are denoted by markers and correlation hole is marked by dotted lines. Pink bold line is the analytical form for GOE (table 4) and the dashed lines are fit using equation 25. The asymptotic values are given in table 2.

The level spacing is scaled as $s = \frac{S}{\langle S \rangle}$ to fix the unit of energy (Appendix A). Then density of NNS for 2×2 O-RPE is [65, 66, 67]

$$P_{\gamma}^{(1)}(s) = 2^{2+\frac{|\gamma|}{2}} f_{\gamma} s e^{-(1+2|\gamma|)f_{\gamma}s^2} I_0((1-2|\gamma|)f_{\gamma}s^2) \quad (5)$$

where $f_{\gamma} = \frac{(\text{EllipticE}(1-2^{-|\gamma|}))^2}{2\pi}$ and $\text{EllipticE}(x) = \int_0^{\frac{\pi}{2}} d\theta \sqrt{1-x\sin^2\theta}$ is the complete elliptic integral. In figure 1(a), $P_{\gamma}^{(1)}(s)$ is shown for various γ where $\gamma = 0$ corresponds to the Gaussian Orthogonal Ensemble (GOE). The Taylor expansion of $P_{\gamma}^{(1)}(s)$ around $s = 0$ apparently implies linear level repulsion irrespective of γ . However, $P_{\gamma}^{(1)}(s)$ attains the maximum around $s^*(\gamma) = (3f_{\gamma}(1+2|\gamma|))^{-\frac{1}{2}}$ where $s^*(\gamma) \rightarrow 0$ in the integrable limit $\gamma \gg 1$ and $P_{\gamma}^{(1)}(s) \rightarrow P_{\text{Poisson}}(s) = \frac{2}{\pi} e^{-\frac{s^2}{\pi}}$. We can fit $P_{\gamma}^{(1)}(s)$ with empirical distributions (e.g. Brody [68], Berry-Robnik [69], Izrailev [70]) to estimate the degree of level repulsion. Nevertheless, such a numerical fit captures the global shape of $P(s)$ without necessarily reflecting the behavior of $P(s \ll 1)$ [71]. To avoid such ambiguity, we compute $\langle s^2 \rangle$, the 2nd moment of NNS, to quantify the exact crossover from level clustering to repulsion. The functional form of $\langle s^2 \rangle$ is given in table 1 and plotted in the inset of figure 1(a). Note that $\langle s^2 \rangle$ is minimum at and symmetric about $\gamma = 0$ (i.e. the GOE limit).

Now we investigate the dynamical properties of 2×2 O-RPE. Given the eigenvectors $|\Phi_1\rangle$ and $|\Phi_2\rangle$ with non-degenerate energies E_1 and E_2 , respectively, we initialize a 2-level system governed by H in any arbitrary initial state $|\Psi_0\rangle \neq |\Phi_{1,2}\rangle$. Then fidelity of the initial state has a periodic time evolution

$$R(t) \equiv |\langle \Psi_0 | e^{-iHt} | \Psi_0 \rangle|^2 = 1 - 4c_1^2 c_2^2 \sin^2 \frac{St}{2} \quad (6)$$

Model	$\langle s^2 \rangle$	$\gamma \rightarrow -\infty$	$\gamma \rightarrow 0$	$\gamma \rightarrow \infty$	$\gamma \rightarrow 0, N \rightarrow \infty$
O-RPE	$\frac{\pi(1+2^{- \gamma })}{2(\text{EllipticE}(1-2^{- \gamma }))^2}$	$\frac{\pi}{2}$	$\frac{4}{\pi} \approx 1.273$	$\frac{\pi}{2}$	1.285
U-RPE	$\frac{\pi(1+2^{\gamma-1})}{(2^{\frac{\gamma}{2}}+c_\gamma)^2}$	$\frac{4}{\pi}$	$\frac{3\pi}{8} \approx 1.178$	$\frac{\pi}{2}$	1.180
S-RPE	$\frac{ 1-2^\gamma (4+2^\gamma)}{2^{\gamma+1}\mu^2}$	$\frac{3\pi}{8}$	$\frac{45\pi}{128} \approx 1.104$	$\frac{\pi}{2}$	1.104
β -RPE	$\langle s^2 \rangle = \frac{2+4\beta\sigma^2}{\mu^2}, \quad \mu = \frac{\beta\Gamma(\frac{\beta}{2})}{\sigma^{\beta}2^{\frac{\beta}{2}}\Gamma(\frac{\beta+1}{2})} {}_2F_1\left(\frac{\beta}{2}, \frac{\beta+2}{2}, \frac{\beta+1}{2}; 1 - \frac{1}{2\sigma^2}\right)$				
β -ensemble	$\langle s^2 \rangle = \frac{(\beta+1)\Gamma(\frac{\beta+1}{2})^2}{2\Gamma(1+\frac{\beta}{2})^2}$				

Table 1. 2nd moment of NNS for 2×2 RPE from various symmetry classes. For S-RPE, μ is given in equation 17. The last column shows $\langle s^2 \rangle$ for the WDE in the thermodynamic limit ($N \rightarrow \infty$), obtained by interpolating numerically evaluated $\langle s^2 \rangle$ from the middle 50% spectrum up to system size, $N = 32768$. For Poisson ensemble, $\langle s^2 \rangle_{N=2} = \frac{\pi}{2}$ and $\langle s^2 \rangle_{N \rightarrow \infty} = 2$.

where $c_j = |\langle \Phi_j | \Psi_0 \rangle|$ i.e. modulus of the overlap of j th eigenstate with $|\Psi_0\rangle$ and $S = |E_2 - E_1|$ determines the periodicity of Rabi oscillation [72]. The fidelity of a general initial state, $|\Psi_0\rangle = \begin{pmatrix} \cos \psi \\ \sin \psi \end{pmatrix}$, is studied in Appendix B. Since we want to identify the crossover from integrability to chaos, let us choose $|\Psi_0\rangle$ as one of the eigenstates in the integrable limit, i.e. $|\Psi_0\rangle = \begin{pmatrix} 1 \\ 0 \end{pmatrix}$. Then for general 2×2 real symmetric matrices, we can express the fidelity as

$$R(t) = 1 - \frac{\sin^2 2\theta}{2} (1 - \cos St) \quad (7)$$

and its ensemble average is given by

$$\langle R(t) \rangle = \bar{R} + \int dS d\theta \frac{\sin^2 2\theta}{2} P(S, \theta) \cos(St). \quad (8)$$

The second term in $\langle R(t) \rangle$ vanishes for $t \gg 1$, hence ensemble averaging suppresses the Rabi oscillation and the fidelity equilibrates to

$$\bar{R} = 1 - \frac{1}{2} \int dS d\theta P(S, \theta) \sin^2 2\theta. \quad (9)$$

It is to be noted that \bar{R} is equivalent to the ensemble averaged Inverse Participation Ratio (IPR, $I = \sum_j |\Phi(j)|^4$). For 2×2 O-RPE, we use the distribution from equation 3 in equation 8 to get the ensemble averaged fidelity

$$\begin{aligned} \langle R(t) \rangle &= \bar{R} + 2^{\frac{\gamma}{2}-3} \int_0^\infty dS \cos(St) f(S) \\ f(S) &= S e^{(c_\gamma - \frac{1}{4})S^2} [I_0(c_\gamma S^2) + I_1(c_\gamma S^2)], \quad -\infty < c_\gamma = \frac{1-2^\gamma}{8} < \frac{1}{8}. \end{aligned} \quad (10)$$

$\langle R(t) \rangle$ is evaluated for different values of γ and is shown in figure 1(b) and the equilibrium value \bar{R} is listed in table 2. Equation 10 implies that for very short time, fidelity

Model	\bar{R}	$\gamma \rightarrow -\infty$	$\gamma \rightarrow 0$	$\gamma \rightarrow \infty$
O-RPE	$1 - \frac{1}{2(1+2^{\frac{\gamma}{2}})}$	$\frac{1}{2}$	$\frac{3}{4}$	1
U-RPE	$\frac{\pi(1+2^{\gamma-1})}{(2^{\frac{\gamma}{2}}+c_\gamma)^2}$	$\frac{1}{2}$	$\frac{2}{3}$	1
S-RPE	$\frac{4^{\gamma+1}+2-3\left(2^\gamma+4^\gamma\frac{\text{sech}^{-1}2^{\frac{\gamma}{2}}}{\sqrt{1-2^{-\frac{\gamma}{2}}}}\right)}{4(2^\gamma-1)^2}$	$\frac{1}{2}$	$\frac{3}{5}$	1
β -RPE	$1 - {}_2F_1\left(\frac{\beta+1}{2}, \frac{\beta+2}{2}; \frac{\beta+3}{2}; 1-2^\gamma\right) \frac{\beta 2^{\frac{\beta\gamma}{2}-1}}{\beta+1}$			
β -ensemble	$1 - \frac{\beta}{2(\beta+1)}$			

Table 2. Asymptotic value of fidelity for 2×2 RPE from various symmetry classes along with limiting cases of γ . For U-RPE, c_γ is given in table 3.

exhibits a quadratic decay, $\langle R(t) \rangle \sim 1 - \frac{t^2}{2\gamma+1}$. After attaining the minimum at Thouless time, t_{Th} , the fidelity grows and asymptotically reach the equilibrium value \bar{R} at the relaxation time, t_R . The gap between the Thouless and the relaxation time is known as the correlation hole. The relative depth of the correlation hole, $\kappa \equiv 1 - \frac{\langle R(t_{\text{Th}}) \rangle}{\bar{R}}$, reflects the long-range energy correlations: $\kappa = 0$ and $\kappa > 0$ implies uncorrelated and correlated spectrum, respectively [8]. In the inset of figure 1(a), we plot κ as a function of γ showing a crossover from integrable to chaotic regime. Note that κ does not show maximum at $\gamma = 0$ but qualitatively reciprocates the crossover observed in $\langle s^2 \rangle$ derived from the eigenvalues only. We also observe that both t_{Th} and t_R increase exponentially as a function of γ , i.e. $\langle R(t) \rangle$ takes longer time to equilibrate while the equilibrium value itself approaches unity as we go towards the integrable limit. Consequently monitoring the fidelity, we can identify the crossover from chaos to integrability in case of 2×2 O-RPE. Such a crossover can be equivalently understood as a deformation of the symmetry present in an integrable Hamiltonian (Appendix C). The fidelities in case of GOE for $N = 2$ and $N \gg 1$ are compared in Appendix D.

3. Unitary Rosenzweig-Porter Ensemble (U-RPE)

Any 2×2 complex hermitian matrix can be expressed as

$$H = \begin{pmatrix} E_1 \cos^2 \theta + E_2 \sin^2 \theta & e^{i\phi} \frac{E_1 - E_2}{2} \sin 2\theta \\ e^{-i\phi} \frac{E_1 - E_2}{2} \sin 2\theta & E_2 \cos^2 \theta + E_1 \sin^2 \theta \end{pmatrix} \quad (11)$$

where the eigenvectors are $|\Phi_1\rangle = \begin{pmatrix} \cos \theta e^{-i\phi} \\ -\sin \theta \end{pmatrix}$ and $|\Phi_2\rangle = \begin{pmatrix} \sin \theta \\ \cos \theta e^{i\phi} \end{pmatrix}$ ignoring a global phase factor of the form $e^{i\alpha}$. The Jacobian of transformation from matrix space to eigenspace is $\frac{\sin 2\theta}{2}(E_1 - E_2)^2$. Proceeding as in the previous section, i.e. starting with equation 1 and integrating over $\phi \in [0, \frac{\pi}{2}]$, we obtain the joint density of eigenvalues and θ for 2×2 U-RPE

$$P(E_1, E_2, \theta) = \frac{2^\gamma}{8\pi} (E_1 - E_2)^2 |\sin 2\theta| e^{-\frac{E_1^2 + E_2^2}{2} + (1-2^\gamma) \frac{(E_1 - E_2)^2}{4} \sin^2 2\theta}. \quad (12)$$

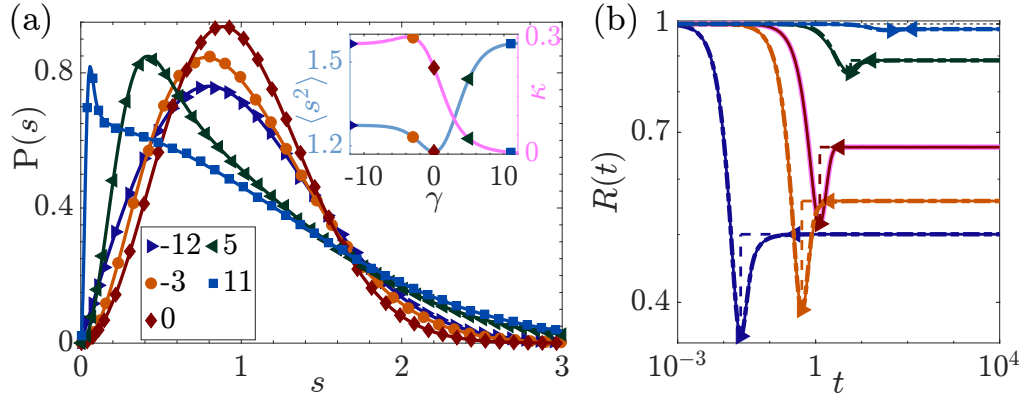


Figure 2. U-RPE: (a) density of NNS for various γ . Solid lines denote analytical form in equation 13 whereas the markers denote simulation over 10^7 samples. Inset shows $\langle s^2 \rangle$, 2nd moment of NNS, where the blue solid line denotes analytical form in table 1 and κ , the relative depth of the correlation hole in the fidelity (pink solid line). (b) temporal evolution of fidelity where Thouless and relaxation times are denoted by markers and correlation hole is marked by dotted lines. Pink bold line is the analytical form for GUE (table 4) and the dashed lines are fit using equation 25. The asymptotic values are given in table 2.

Then using equation 4, we get the density of NNS for 2×2 U-RPE [73]

$$P_{\gamma}^{(2)}(s) = \frac{2\mu^2}{\sqrt{|1-2\gamma|}} s e^{-\mu^2 s^2} g(\mu\sqrt{|1-2\gamma|}s) \quad (13)$$

where $\mu = \frac{2^{\frac{\gamma}{2}} + c_{\gamma}}{\sqrt{\pi}}$ and the functional forms of c_{γ} and $g(x)$ are given in table 3. $P_{\gamma}^{(2)}(s)$ for various γ are shown in figure 2(a) where $\gamma = 0$ corresponds to the Gaussian Unitary Ensemble (GUE). Equation 13 implies that 2×2 U-RPE exhibits quadratic (linear) level repulsion for $\gamma \rightarrow 0$ ($\gamma \rightarrow -\infty$). We present the 2nd moment of NNS in table 1 and plot the same in the inset of figure 2(a) to show a crossover from linear to quadratic to no level repulsion. Having quantified the degree of level repulsion, here again we focus on the dynamical properties of 2×2 U-RPE. We prepare the system in the initial state $|\Psi_0\rangle = \begin{pmatrix} 1 \\ 0 \end{pmatrix}$. The eigenvectors $|\Phi_{1,2}\rangle$ imply that the ensemble averaged fidelity of $|\Psi_0\rangle$ in a hermitian system is generically given by equation 8 and particularly for U-RPE, we

	c_{γ}	$g(s)$	$f(s)$
$\gamma < 0$	$\frac{\cos^{-1}\left(2^{\frac{\gamma}{2}}\right)}{\sqrt{1-2\gamma}}$	$\text{Erf}(s)$	$\frac{\sqrt{\pi}}{2} \frac{(2s^2-1)\text{Erf}(s)e^{s^2}}{s} + 1$
$\gamma \geq 0$	$\frac{\cosh^{-1}\left(2^{\frac{\gamma}{2}}\right)}{\sqrt{2^{\gamma}-1}}$	$\text{Erfi}(s)$	$\frac{(2s^2+1)\text{Df}(s)}{s} - 1$

Table 3. U and S-RPE: $c_{\gamma}, g(s)$ for $P_{\gamma}^{(2)}(s)$ (equation 13) and $f(s)$ for $P_{\gamma}^{(4)}(s)$ (equation 17).

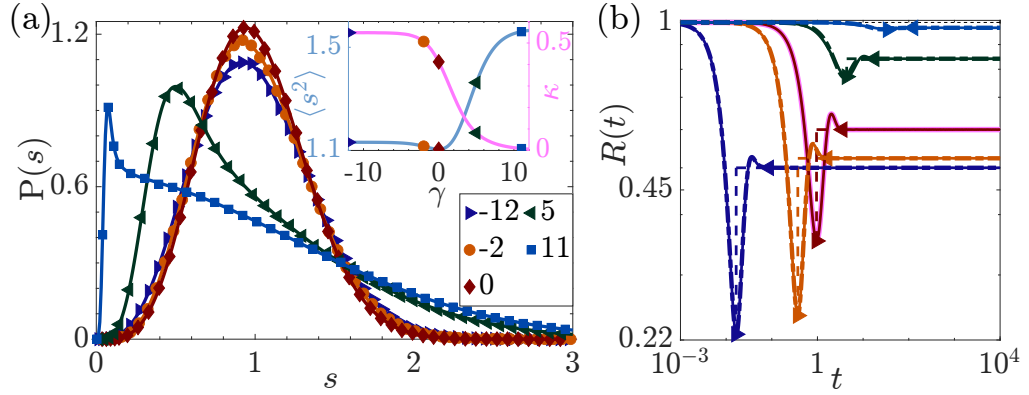


Figure 3. S-RPE: (a) density of NNS for various γ . Solid lines denote analytical form in equation 17 whereas the markers denote simulation over 10^7 samples. Inset shows $\langle s^2 \rangle$, 2nd moment of NNS, where the blue solid line denotes analytical form in table 1 and κ , the relative depth of the correlation hole in the fidelity (pink solid line). (b) temporal evolution of fidelity where Thouless and relaxation times are denoted by markers and correlation hole is marked by dotted lines. Pink bold line is the analytical form for GSE (table 4) and the dashed lines are fit using equation 25. The asymptotic values are given in table 2.

obtain

$$\begin{aligned} \langle R(t) \rangle &= \bar{R} + \frac{e^{-t^2}}{2(2^{-\gamma} - 1)} + \frac{2^{\gamma-1}}{\sqrt{1-2^{-\gamma}}} \int_0^\infty dS \cos(St) f(S) \\ f(S) &= e^{-2^{\gamma-2} S^2} \text{Erf} \left(\frac{\sqrt{1-2^{-\gamma}}}{2} S \right) \left(\frac{S}{2} - \frac{1}{(1-2^{-\gamma})S} \right) \end{aligned} \quad (14)$$

where \bar{R} is given in table 2 and is trivially equal to the ensemble averaged IPR. In figure 2(b), we show the temporal evolution of fidelity for various γ . Equation 14 implies that for very short time ($t \ll 1$), fidelity decays as $\langle R(t) \rangle = 1 - \frac{t^2}{2^\gamma}$ while κ captures the crossover from chaotic to integrable regime, as shown in the inset of figure 2(a).

4. Symplectic Rosenzweig-Porter Ensemble (S-RPE)

Now we study the symplectic ensemble to complete Dyson's threefold classification of the symmetry classes [2] in case of RPE. A 2×2 symplectic matrix is defined in terms of quaternions as

$$\begin{aligned} H &= \begin{pmatrix} \hat{h}_{11} & \hat{h}_{12} \\ \hat{h}_{21} & \hat{h}_{22} \end{pmatrix}, \quad \hat{h}_{mn} = \vec{h}_{mn} \cdot \vec{\tau} \\ \vec{h}_{mn} &= \{h_{mn}^{(0)}, h_{mn}^{(1)}, h_{mn}^{(2)}, h_{mn}^{(3)}\}, \quad \vec{\tau} = \{\mathbb{I}, -i\sigma^x, -i\sigma^y, -i\sigma^z\} \end{aligned} \quad (15)$$

where $\sigma^{x,y,z}$ are the Pauli matrices and \mathbb{I} is the identity matrix. H has two unique eigenvalues with 2-fold Kramer's degeneracy [74]. As H is hermitian, $h_{mn}^{(j)} = h_{nm}^{(j)} \in \mathbb{R} \forall j$, leading to six independent real elements. The eigenvectors of H form a unitary matrix $U \equiv U(\zeta, \alpha, \theta, \phi)$ dependent on four independent elements. Then using the

change of variables in table E1, we can express the joint density of non-degenerate energies and ζ in case of 2×2 S-RPE

$$P(E_1, E_2, \zeta) = \frac{4^{\gamma+1}}{2^9 \pi} |\sin \zeta|^3 (E_1 - E_2)^4 e^{-\frac{E_1^2 + E_2^2}{2} + (1-2\gamma) \frac{(E_1 - E_2)^2}{4} \sin^2 \zeta} \quad (16)$$

where ζ plays the role of 2θ in case of O and U-RPE. For $\gamma = 0$, we retrieve the Gaussian Symplectic Ensemble (GSE). Integrating out ζ in equation 16 yields the joint density of energy and using equation 4, we get the density of NNS for 2×2 S-RPE

$$P_\gamma^{(4)}(s) = \frac{2^{2\gamma+1} \mu^3}{\sqrt{\pi} |1-2\gamma|^5} s^2 \exp\left(-\frac{\mu^2 s^2}{|1-2\gamma|}\right) f(\mu s) \quad (17)$$

$$\mu = \frac{1}{\sqrt{\pi} |1-2\gamma|} \left| \frac{3}{2} - 2^\gamma - 2^{\frac{\gamma}{2}} \left(2 - \frac{3}{2^{\gamma+1}}\right) c_\gamma \right|$$

where $f(x)$ and c_γ are given in table 3. $P_\gamma^{(4)}(s)$ exhibits cubic ($\gamma \rightarrow -\infty$), quartic ($\gamma = 0$) or no ($\gamma \rightarrow \infty$) level repulsion depending on γ . Note that in 2×2 RPE from all the three symmetry classes, the degree of level repulsion for $\gamma \rightarrow -\infty$ is precisely one less than that in the Wigner-Dyson (i.e. $\gamma = 0$) limit. We show the 2nd moment of NNS in table 1 and plot the same in the inset of figure 3(a) to show a crossover among various degrees of level repulsion.

Proceeding as in the previous sections, average fidelity of $|\Psi_0\rangle$ for 2×2 S-RPE becomes

$$\langle R(t) \rangle = \bar{R} + \frac{2^{2\gamma-3}}{\sqrt{\pi}} \int_0^\infty dS \cos(St) f(S) \quad (18)$$

$$f(S) = \frac{(2^\gamma - 1)s^3 + 4s + \frac{12}{s(2^\gamma-1)}}{(2^\gamma - 1)^{\frac{3}{2}}} - \frac{s^2 + \frac{6}{2^\gamma-1}}{2^\gamma - 1}$$

where \bar{R} is given in table 2. Here also κ captures the crossover from chaotic to integrable regime, as shown in the inset of figure 3(a). Importantly, a 2×2 self-dual matrix from S-RPE has two-fold Kramers' degeneracy and dimension 4 in the computational basis, hence the ensemble averaged IPR does not coincide with \bar{R} .

Model	$P(s)$	$\langle R(t) \rangle$
Poisson	$\frac{2}{\pi} e^{-\frac{s^2}{\pi}}$	1
GOE	$\frac{\pi}{2} s e^{-\frac{\pi}{4} s^2}$	$1 - \frac{1}{2} t D_F(t)$
GUE	$\frac{32}{\pi^2} s^2 e^{-\frac{4}{\pi} s^2}$	$\frac{2}{3} + \frac{1}{3} (1 - 2t^2) e^{-t^2}$
GSE	$\frac{2^{18}}{3^6 \pi^3} s^4 e^{-\frac{64}{9\pi} s^2}$	$\frac{3}{5} + \frac{1}{15} (6 + 8t^2 (t^2 - 3)) e^{-t^2}$
β -ensemble	$a_\beta s^\beta e^{-b_\beta^2 s^2}$	$\bar{R} + (1 - \bar{R}) {}_1F_1\left(\frac{\beta+1}{2}; \frac{1}{2}; -t^2\right)$

Table 4. Poisson, Wigner-Dyson and β -ensemble: Density of NNS and mean fidelity, where $D_F(x) = e^{-x^2} \int_0^x e^{y^2} dy = \frac{\sqrt{\pi}}{2} e^{-x^2} \text{Erfi}(x)$ is the Dawson integral. For β -ensemble, $a_\beta = \frac{2\Gamma(1+\frac{\beta}{2})^{\beta+1}}{\Gamma(\frac{\beta+1}{2})^{\beta+2}}$ and $b_\beta = \frac{\Gamma(1+\frac{\beta}{2})}{\Gamma(\frac{\beta+1}{2})}$ in the density of NNS and $\bar{R} = 1 - \frac{\beta}{2(\beta+1)}$ in the average fidelity. Note that β -ensemble encompasses the results for Poisson and WDE for respective values of β .

5. β -Rosenzweig-Porter Ensemble (β -RPE)

So far we have studied the density of NNS and the average fidelity in case of RPE from three symmetry classes consisting of real, complex and quaternion matrices where the Dyson's index, β can be only 1, 2 and 4, respectively and γ controls the disorder strength. Particularly for $\gamma = 0$, we get closed form expressions for the $\langle R(t) \rangle$ of GOE, GUE, GSE (table 4). Now we allow β to be any real number such that the joint density of eigenvalues follows the β -ensemble [76, 77]. Various canonically invariant matrix models of β -ensemble are proposed till date [78, 79, 80]. However, a convenient matrix representation of β -ensemble can be found at the cost of canonical invariance, where the relevant ensemble consists of random real symmetric tridiagonal matrices [63]. Such a matrix model hosts three distinct phases separated by two 2nd order critical points [81, 82]. We can further generalize β -ensemble if we let the relative strength of diagonal and off-diagonal elements to vary. In a simple two-level set-up, we introduce a two-parameter ensemble of 2×2 real matrices, the β -Rosenzweig-Porter ensemble (β -RPE):

$$H = \begin{pmatrix} x & z \\ z & y \end{pmatrix}, \quad x, y \sim \mathcal{N}(0, 1), \quad \frac{z}{\sigma} \sim \chi_\beta, \quad \sigma^2 = \frac{1}{2^{\gamma+1}} \quad (19)$$

where χ_β is the chi distribution with degree of freedom β and x, y, z are mutually independent. Thus in β -RPE, γ controls the relative strength of the disorder and β is the fictitious inverse temperature of the analogous Coulomb gas model [83]. We will show that β -RPE encompasses all the results given for previous RPEs. Equation 19 implies that the density in matrix space is

$$P(H) = \frac{1}{\sigma^\beta 2^{\frac{\beta}{2}} \pi \Gamma(\frac{\beta}{2})} z^{\beta-1} \exp\left(-\frac{x^2 + y^2 + \frac{z^2}{\sigma^2}}{2}\right) \quad (20)$$

Since H in equation 19 is a real symmetric matrix, corresponding eigenvectors parameterized by θ forms an orthogonal (rotation) matrix and H can be expressed in terms of the energies, $E_{1,2}$ and θ as in equation 2. However, the off-diagonal element z is always positive, hence $\theta \in [0, \frac{\pi}{2}]$ for $E_1 \geq E_2$ and $\theta \in (\frac{\pi}{2}, \pi]$ for $E_1 < E_2$. Then we can transform the density in matrix space (equation 20) to the density in eigenspace

$$P(E_1, E_2, \theta) = \frac{|E_1 - E_2|^\beta |\sin 2\theta|^{\beta-1}}{\sigma^\beta 2^{\frac{3\beta}{2}} \pi \Gamma(\frac{\beta}{2})} e^{-\frac{E_1^2 + E_2^2}{2} + (1 - \frac{1}{2\sigma^2}) \frac{\sin^2 2\theta}{4} (E_1 - E_2)^2}. \quad (21)$$

Note that other than the normalization constant, $P(E_1, E_2, \theta)$ matches with those of O, U and S-RPE (equation 3, 12 and 16) for respective values of β . Integrating out θ in equation 21 gives the joint density of energies, allowing us to compute the density of NNS

$$\begin{aligned} P_\gamma^{(\beta)}(s) &= \mu f(\mu s) \\ f(s) &= \frac{2^{\frac{\beta}{2}(\gamma-2)}}{\Gamma(\frac{\beta+1}{2})} S^\beta e^{-\frac{s^2}{4}} {}_1F_1\left(\frac{\beta}{2}; \frac{\beta+1}{2}; (1-2^\gamma) \frac{S^2}{4}\right) \\ \mu &= \frac{2^{\frac{\beta\gamma}{2}} \beta \Gamma(\frac{\beta}{2})}{\Gamma(\frac{\beta+1}{2})} {}_2F_1\left(\frac{\beta}{2}, \frac{\beta+2}{2}; \frac{\beta+1}{2}; 1-2^\gamma\right) \end{aligned} \quad (22)$$

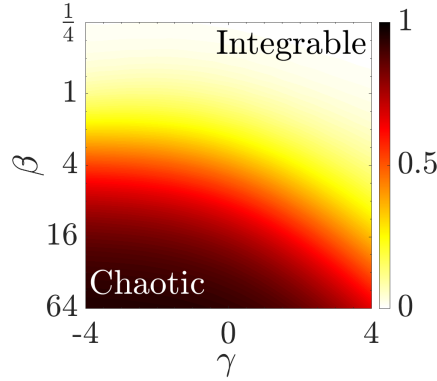


Figure 4. β -RPE: κ , relative depth of the correlation hole in the γ - β plane showing the crossover between chaotic and integrable regime.

where ${}_1F_1(a; b; z)$ is the Kummer confluent hypergeometric function and ${}_2F_1(a, b; c; z)$ is the hypergeometric function. $P_\gamma^{(\beta)}(s)$ converges to the density of NNS for O, U and S-RPE (equation 5, 13, 17) for $\beta = 1, 2$ and 4, respectively, while for $\gamma = 0$, we get the generalized Gamma distribution valid for 2×2 β -ensemble [84]. The 2nd moment of NNS for β -RPE is given in table 1.

To understand the unitary time evolution of the state $|\Psi_0\rangle = \begin{pmatrix} 1 \\ 0 \end{pmatrix}$, we apply equation 7 to equation 21 to get the ensemble averaged fidelity

$$\begin{aligned} \langle R(t) \rangle &= \bar{R} + \frac{\beta 2^{\frac{\beta\gamma}{2}-3}}{\Gamma(\frac{\beta+3}{2})} \int_0^\infty dS \cos(St) f(S) \\ f(S) &= S^\beta e^{-\frac{S^2}{4}} {}_1F_1\left(\frac{\beta+2}{2}; \frac{\beta+3}{2}; (1-2\gamma) \frac{S^2}{4}\right) \end{aligned} \quad (23)$$

where \bar{R} is given in table 2. Equation 23 yields the fidelity for O, U and S-RPE (equation 10, 14, 18) for respective values of β . For very short time, average fidelity of β -RPE decays as $\langle R(t) \rangle \sim 1 - \beta\sigma^2 t^2$. Since the relative depth of the correlation hole, κ , depends on both energy and state structure, we show κ in the γ - β plane in figure 4 to identify a crossover between chaotic and integrable regimes.

For $\gamma = 0$, we obtain a closed form valid for 2×2 β -ensemble

$$\langle R(t) \rangle = \bar{R} + (1 - \bar{R}) {}_1F_1\left(\frac{\beta+1}{2}; \frac{1}{2}; -t^2\right), \quad \bar{R} = 1 - \frac{\beta}{2(\beta+1)} \quad (24)$$

We observe that β , the degree of level repulsion, appears as the only parameter in equation 24. Hence for any 2×2 matrix from any symmetry class, we propose a two parameter ansatz for the fidelity of the initial state $|\Psi_0\rangle$ to follow

$$\frac{R(a, b; t) - \bar{R}}{1 - \bar{R}} = {}_1F_1\left(\frac{b+1}{2}; \frac{1}{2}; -a^2 t^2\right) \quad (25)$$

where a scales the time axis and b controls the rate of initial decay of the fidelity. In figures 1, 2 and 3(b), we show that equation 25 provides a good fit for the fidelity for all values of γ across any symmetry class. Thus similar to Brody distribution serving as an

empirical form of density of NNS, our ansatz in equation 25 works as a fitting function for fidelity of any 2-level system.

6. Rosenzweig-Porter Ensemble for large N

In this section, we numerically compute the statistical and dynamical properties of RPE for large matrix dimensions, N

$$\langle H_{n,n}^2 \rangle = 1, \quad \langle |H_{n,m}|^2 \rangle = \frac{\beta}{2N\gamma}, \quad \gamma \in \mathbb{R}, \quad (26)$$

and compare them with those of 2×2 systems obtained earlier. The density of NNS for 2×2 WDE (RPE with $\gamma = 0$) is a good approximation for that of the larger matrices from the same ensemble [74], consequently 2nd moment of NNS for $N = 2$ and large N are close to each other (table 1). However, this is not true for the RPE with $\gamma \neq 0$ since in 2×2 RPE, the density of NNS interpolates between clustering $P(s) \sim e^{-s^2}$ and repulsion $P(s) \sim s^\beta e^{-s^2}$ whereas for $N \gg 1$, the clustering is of the form $P(s) = e^{-s}$ in the integrable limit. In figure 5(a), (b) and (c), we show the densities of NNS of the unfolded eigenvalues (from the middle 25% of the spectrum averaged over 128 disordered realizations for $N = 4096$) for various γ values along with the analytical expressions of the 2×2 WDE and Poisson ensemble. To identify the transition from level repulsion to clustering, we show the 2nd moment of NNS as a function of γ for various N in figure 5(d), (e) and (f). The crossover curves get steeper with N and tend to intersect each other around $\gamma = 2$. Using the 2nd order phase transition ansatz [81], we are able to collapse the $\langle s^2 \rangle$ data from all system sizes, as shown in the respective insets. Therefore, short-range energy correlations for RPE from all the three symmetry classes show a 2nd order phase transition at $\gamma = 2$, which was previously established using ratio of level spacing [37].

Having shown the statistical measure of chaos-integrability transition in RPE, we now look at the corresponding dynamical signatures. For $|\Psi\rangle$, the δ -localized states with energy close to 0 (i.e. $\langle \Psi | H | \Psi \rangle \sim 0$), we compute the ensemble averaged time evolution of the fidelity

$$\langle R(t) \rangle = |\langle \Psi | \Psi(t) \rangle|^2 = \sum_{m,n} |c_m|^2 |c_n|^2 e^{i(E_m - E_n)t} \quad (27)$$

where $c_n = \langle E_n | \Psi \rangle$ is the n th component of $|\Psi\rangle$ in the energy eigenbasis $\{|E_n\rangle\}$. Equation 27 implies that the asymptotic value of fidelity is $\bar{R} = \sum_n |c_n|^4$, which is the IPR of the initial state in $\{|E_n\rangle\}$, provided the energy spectrum is non-degenerate [75]. However, self-dual quaternion matrices from S-RPE show two-fold Kramers' degeneracy, hence the asymptotic value of fidelity becomes

$$\bar{R}_{\text{S-RPE}} = \sum_n |c_n|^4 + 2 \sum_{m=1,3,5,\dots} |c_m c_{m+1}|^2. \quad (28)$$

Therefore, degeneracy in the energy spectrum increases the asymptotic value of fidelity, i.e. an initially localized excitation spreads over larger fraction of the total Hilbert space

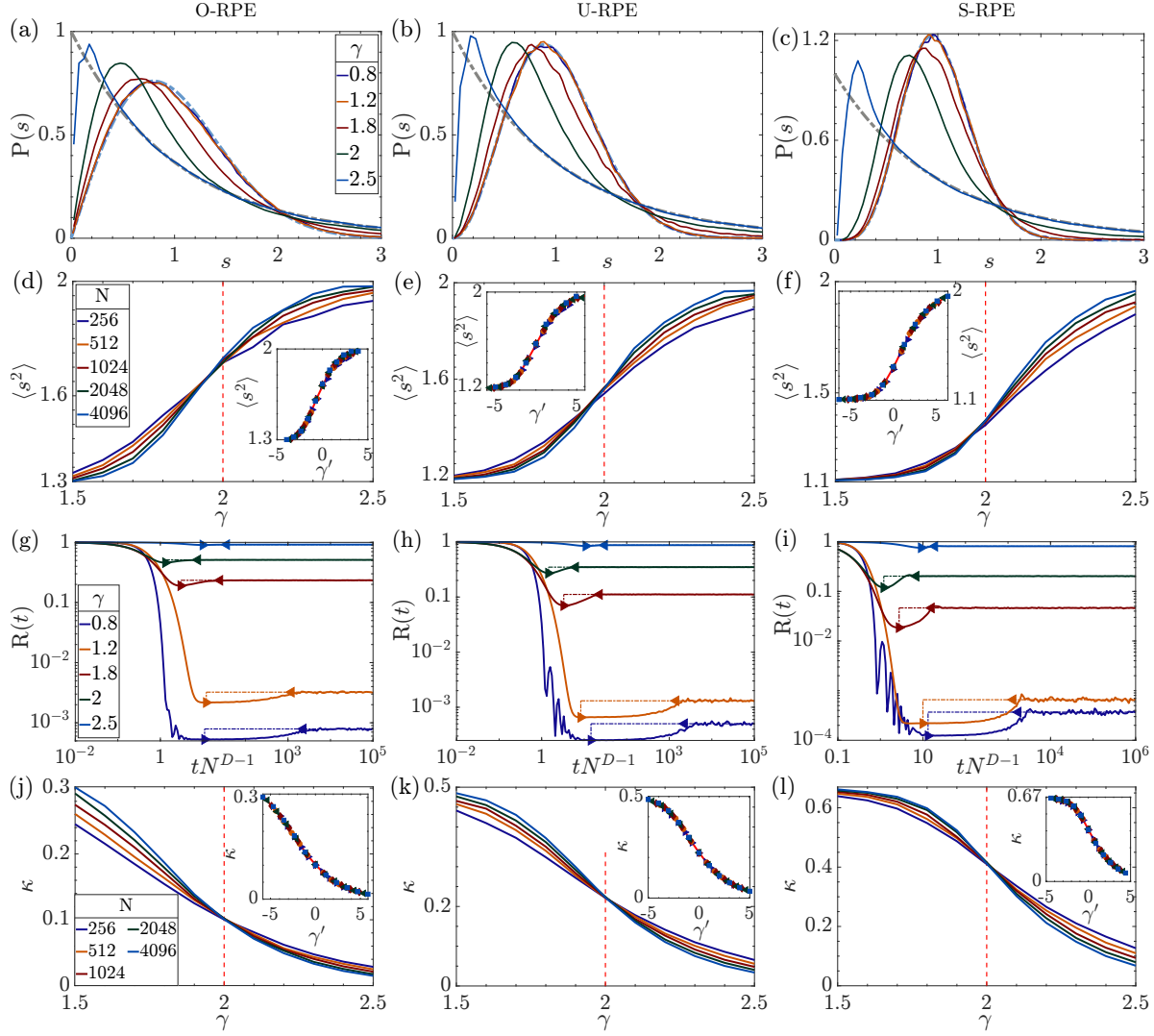


Figure 5. RPE for large N : 1st, 2nd and 3rd columns show the results for orthogonal, unitary and symplectic Rosenzweig-Porter Ensemble, respectively. Densities of NNS of the unfolded eigenvalues (obtained from middle 25% of the spectrum) are shown for varying γ values in (a), (b) and (c) ($N = 4096$). Dashed lines denote the analytical curves for 2×2 WDE and Poisson ensemble. In (d), (e) and (f), the 2nd moment of NNS is shown for varying N . In (g), (h) and (i), we show the time evolution of the fidelity of $\frac{N}{4}$ δ -localized states with energy closest to 0 for various γ and $N = 4096$. Dashed lines denote the equilibrium values and markers denote the Thouless and relaxation times. In (j), (k) and (l), κ , the relative depth of the correlation hole is shown for varying N . The insets of (d), (e), (f), (j), (k) and (l) show the collapsed data using 2nd order phase transition ansatz, $\gamma' = (\gamma - 2)(\log N)^{\frac{1}{\nu}}$ [81]. The estimated critical exponent $\nu \approx 1.2025, 0.988, 0.9765$ for $\langle s^2 \rangle$ and $\nu \approx 1.0102, 1.0745, 1.1414$ for κ from the three symmetry classes, respectively. The data are averaged over 128 disorder realizations.

volume at long time. In figure 5(g), (h) and (i), we show the time evolution of the ensemble averaged fidelity for RPE from all the three symmetry classes for $N = 4096$ and various values of γ . We also mark the Thouless and relaxation times in each case and show the asymptotic value of fidelity via dashed lines. Note that, the Thouless time

increases with system size as $t_{\text{Th}} \propto N^{1-D}$ where D is the typical fractal dimension of the bulk eigenstates [44]. Hence, in the non-ergodic ($1 < \gamma < 2$, $D = 2 - \gamma$) and localized ($\gamma \geq 2$, $D = 0$) regimes, the Thouless time increases exponentially with system size and we scale the time axis as $t \rightarrow tN^{D-1}$. The relative depths of the correlation hole are shown in figure 5(j), (k) and (l) as a function of γ for various N . Corresponding insets show the collapsed data implying a 2nd order phase transition from chaos to integrability at $\gamma = 2$ for RPE from all the three symmetry classes. Therefore, κ is a robust measure of dynamical signature of chaos-integrability crossover, which is particularly important for experiments with lack of knowledge of the energy levels [86].

7. Conclusions

In this work, we study the energy correlations and the dynamical properties of 2×2 generalized random matrix ensembles. In each of the Dyson's threefold classifications, i.e. orthogonal, unitary and symplectic symmetry classes, we derive an analytical expression of the density and 2nd moment of NNS from the eigenvalue statistics for 2×2 RPE. As the disorder strength (γ) is varied, the 2nd moment (table 1) provides an exact quantification of the crossover among various degrees of level repulsion providing a better method than any empirical fitting. A general matrix model, β -RPE, has been introduced, where in addition to the disorder strength, the Dyson index, β , can be varied continuously such that β -RPE reproduces the results of the above symmetry classes for $\beta = 1, 2$ and 4 . In such a generalized matrix model, our aim has been to determine the crossover in the two-parameter (γ, β) phase plane in terms of both spectral and dynamical properties.

In order to study the dynamics, we prepare our two-level systems in the eigenstate of an integrable Hamiltonian and look at the time evolution of the corresponding fidelity. Any non-degenerate 2-level system undergoes Rabi oscillation if not prepared in its eigenstate [72]. However, ensemble averaging suppresses the Rabi oscillation, and the average fidelity, $\langle R(t) \rangle$ relaxes to an equilibrium value \bar{R} , as ensemble averaging for a fixed initial state is equivalent to a mixed-unitary quantum channel destroying the coherence in the energy eigenbasis [85]. For the general β -RPE, we analytically obtain the temporal evolution of $\langle R(t) \rangle$ which reduces to simpler expressions (table 4) for the above-mentioned symmetry classes. We observe that upon increasing the system parameter γ (therefore reducing the relative strength of hopping disorder) in any RPE, ensemble averaged fidelity takes longer time to equilibrate while the equilibrium value, \bar{R} , approaches unity. In general, $\langle R(t) \rangle$, after an initial quadratic decay, exhibits a minimum at Thouless time and equilibrates to \bar{R} with a characteristic relaxation time-scale. We propose an ansatz (equation 25) for the average fidelity of any 2-level system, therefore providing an empirical expression characterizing the dynamical crossover from chaos to integrability. We numerically estimate the relative depth of the correlation hole, which quantifies the crossover in qualitative agreement with that observed in the second moment of NNS. Such a crossover in β -RPE can be physically understood as the

manifestation of the deformation of the symmetry present in an integrable Hamiltonian. In spite of the analytical simplicity of 2×2 β -RPE, corresponding $\langle R(t) \rangle$ captures the generic dynamical feature observed in large dimensional random matrices and realistic spin Hamiltonians [8, 9, 75, 86, 87]. We have also numerically computed the 2nd moment of NNS and the fidelity for large N and obtain qualitatively identical features as shown for 2×2 RPE. We find that both the 2nd moment of NNS and the relative depth of the correlation hole exhibit a second order phase transition at $\gamma = 2$.

Our results can be used to understand the fidelity of information transfer in a pre-engineered quantum wire. Note that a d -dimensional Cartesian product of a linear chain of two qubits governed by the Pauli matrix $\hat{\sigma}_x$ in the first excitation subspace allows perfect transfer of excitation between the antipodal points of the resulting hypercube geometry for any d [88, 89]. Therefore, a Cartesian product of two-qubit chains governed by RPE may present a novel mechanism for controlling the transfer fidelity. Another interesting problem will be to consider a dimer governed by an electronic Hamiltonian from 2×2 RPE and place it in a monochromatic quantized electromagnetic cavity to achieve a generalization of the Jaynes-Cummings model [51], where controlling the extent of integrability of the dimer Hamiltonian may affect the population dynamics in a non-trivial manner. Therefore, our dynamical characterization of the loss of integrability in generalized matrix ensembles can have many potential applications.

Acknowledgment: AKD is supported by an INSPIRE Fellowship, DST, India and the Fulbright-Nehru grant no. 2879/FNDR/2023-2024.

Author contribution statement: AKD and AMG performed the analysis and wrote the paper.

Appendix A. Global scaling vs. unfolding

To obtain a universal form of the energy correlations for $N \gg 1$, the eigenvalues need to be unfolded to get rid of the global shape of the density of states [90]. However for $N = 2$, mean level spacing has the same order of magnitude as the global bandwidth, hence the eigenvalues fluctuate around their mean positions in the same length scale as the global bandwidth. Therefore, unfolding leads to loss of universality for two-level systems. For example, unfolding in case of the Poisson ensemble yields $P(s)_{N=2} = 1 - \frac{s}{2}$, $s \in [0, 2]$ whereas $P(s) = e^{-s}$ in the thermodynamic limit ($N \rightarrow \infty$). Hence for 2-level systems, we use the global scaling $s = \frac{S}{\langle S \rangle}$ to enforce $\int_0^\infty ds P(s) = 1$ (normalization) and $\int_0^\infty ds sP(s) = 1$ (i.e. $\langle s \rangle = 1$). This ensures that Wigner's surmise is obtained for 2×2 GOE whereas unfolding produces a significantly different from [67].

Appendix B. Fidelity of a general state for O-RPE

Recall that the eigenvectors of a real symmetric matrix constitute a rotation matrix parameterized by θ . Then for an initial state, $|\Psi_0\rangle = \begin{pmatrix} \cos \psi \\ \sin \psi \end{pmatrix}$, the fidelity becomes $R(t) = 1 - \sin^2(2\theta + 2\psi) \sin^2 \frac{St}{2}$ where $S = |E_2 - E_1|$. Then for 2×2 O-RPE, ensemble averaged fidelity is

$$\begin{aligned} \langle R(t) \rangle &= \bar{R} + 2^{\frac{\gamma}{2}-3} \int_0^\infty dS \cos(St) f(S) \\ f(S) &= S e^{(c_\gamma - \frac{1}{4})S^2} [I_0(c_\gamma S^2) + I_1(c_\gamma S^2) \cos 4\psi] \\ \bar{R} &= \frac{3}{4} + \frac{\cos 4\psi}{4} \left(1 - \frac{2}{1 + 2^{\frac{\gamma}{2}}} \right) \end{aligned} \quad (\text{B.1})$$

which is a slightly modified version of equation 10. Equation B.1 implies that $\langle R(t) \rangle$ is independent of the initial state for $\gamma = 0$ (i.e. GOE limit) which can be attributed to the orthogonal invariance present at $\gamma = 0$. Due to 4ψ appearing in the argument of

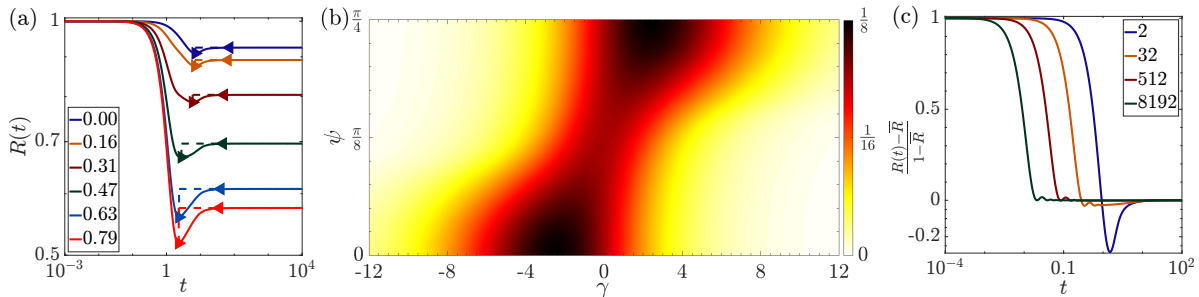


Figure B1. (a) Ensemble averaged fidelity for 2×2 O-RPE for $\gamma = 5$ and different initial states parameterized by ψ (equation B.1). Thouless and relaxation times are shown via marker and the correlation hole is marked by dashed lines. (b) κ , the relative depth of correlation hole for 2×2 O-RPE in γ - ψ plane. (c) GOE, scaled fidelity for various $N > 2$ [87] and $N = 2$ (Table 4).

cosine function, we only need to look at $0 \leq \psi \leq \frac{\pi}{4}$ where $|\Psi_0\rangle$ changes from $\begin{pmatrix} 1 \\ 0 \end{pmatrix}$ to $\frac{1}{\sqrt{2}} \begin{pmatrix} 1 \\ 1 \end{pmatrix}$. In figure B1(a), we show the mean fidelity for various initial states for $\gamma = 5$ while κ , the relative depth of the correlation hole is shown in figure B1(b). However, κ is a measure of integrability only for $\psi = 0$ where $|\Psi_0\rangle$ is an eigenstate of the integrable systems.

Appendix C. RPE as deformed ensemble

In RPE, all the symmetries present in an integrable Hamiltonian is broken in a mean-field manner. Hence RPE can be thought as a deformed ensemble. This can be easily illustrated in case of $N = 2$. Any 2×2 matrix from O-RPE can be written as

$$H = H_+ + 2^{-\frac{\gamma}{2}} H_-, \quad H_+ = y\mathbb{I} + z\sigma_z, \quad H_- = x\sigma_x \quad (\text{C.1})$$

where x, y, z are mutually independent and follow $\mathcal{N}(0, \frac{1}{2})$, i.e. Gaussian distribution with mean 0 and variance $\frac{1}{2}$. Since $\{\sigma_x, \sigma_z\} = 0$, the symmetry present in H_+ is deformed by H_- where γ controls the perturbation strength. Note that the perturbation strength diverges for $\gamma \rightarrow -\infty$, leading to inflation of eigenvalues as in the Pechukas-Yukawa gas [91]. Therefore we can regularize the O-RPE following [92]

$$H = \cos \alpha H_+ + \sin \alpha H_-$$

$$\Rightarrow P(S, \theta) = \frac{S}{\pi \sin 2\alpha} e^{-\left(\frac{\sin^2 2\theta \cot 2\alpha}{\sin 2\alpha} + \frac{1}{4 \cos^2 \alpha}\right) S^2} \quad (\text{C.2})$$

where S is the energy gap and θ parameterizes the eigenstates. Equation C.2 ensures that the eigenvalues are always bounded.

Alternatively, starting from a general symmetry operator, \mathbb{O} , we can obtain the integrable Hamiltonian and its symmetry breaking counterpart (table C1). Then we can define $H(\lambda) = H_+ + \lambda H_-$, where λ controls the perturbation strength. $H(\lambda)$ can be mapped to RPE as we identify the perturbation strength as the variance of

\mathbb{O}	H_+	H_-
$\begin{pmatrix} \cos \xi & \sin \xi \\ \sin \xi & -\cos \xi \end{pmatrix}$	$\begin{pmatrix} x & \frac{\tan \xi}{2}(x-z) \\ \frac{\tan \xi}{2}(x-z) & z \end{pmatrix}$	$y \begin{pmatrix} -\tan \xi & 1 \\ 1 & \tan \xi \end{pmatrix}$
$\begin{pmatrix} \cos \xi & \sin \xi e^{-i\alpha} \\ \sin \xi e^{i\alpha} & -\cos \xi \end{pmatrix}$	$\begin{pmatrix} x & \frac{\tan \xi}{2}(x-z)e^{-i\alpha} \\ \frac{\tan \xi}{2}(x-z)e^{i\alpha} & z \end{pmatrix}$	$\begin{pmatrix} -u \cos \phi' \tan \xi & v + iw \\ v - iw & u \cos \phi' \tan \xi \end{pmatrix}$

Table C1. Structures of the symmetry operator \mathbb{O} , integrable Hamiltonian, H_+ and the symmetry breaking Hamiltonian H_- where first and second row corresponds to symmetric and hermitian matrices, respectively. In the diagonalizing basis of \mathbb{O} , we can reduce the symmetric matrices as: $H_+ \rightarrow \frac{x+z}{2}\mathbb{I} + \frac{x-z}{2}\sigma_z$ and $H_- \rightarrow y \sec \xi \sigma_x$. For hermitian H_- , $u = \sqrt{v^2 + w^2}$, $\phi' = \alpha + \phi$ and $\phi = \tan^{-1} \frac{w}{v}$.

	$\langle R(t \ll 1) \rangle$	Γ	$\langle R(t \gg 1) \rangle$	t_{Th}	$R(t_{\text{Th}})$	t_{R}	\bar{R}	κ
$N = 2$	$1 - \frac{t^2}{2}$	$\sqrt{\frac{3}{2}}$	$\bar{R} - \frac{1-\bar{R}}{2t^2}$	1.50198	0.678813	$\sqrt{\frac{1}{6\epsilon}}$	$\frac{3}{4}$	0.0949
$N \gg 1$	$1 - Nt^2$	\sqrt{N}	$\bar{R} - \frac{1-\bar{R}}{3t^2}$	$\left(\frac{3}{\pi}\right)^{\frac{1}{4}} \approx 0.9885$	$\frac{2}{N}$	$\frac{1}{3}\sqrt{\frac{N}{\epsilon}}$	$\frac{3}{N}$	$\frac{1}{3}$

Table D1. Ensemble averaged fidelity in GOE: comparison between $N = 2$ and $N \gg 1$. Γ is the width of the LDOS and $\kappa \equiv 1 - \frac{\langle R(t_{\text{Th}}) \rangle}{\bar{R}}$ is the relative depth of correlation hole. t_{R} , the relaxation time is defined as the point where $\langle R(t) \rangle$ approaches the ϵ -neighborhood of the equilibrium value, \bar{R} , where $\epsilon \ll 1$ is the tolerance value. For example, $\epsilon = 10^{-3} \Rightarrow t_{\text{R}} \approx 13$ for $N = 2$.

off-diagonal elements in RPE. Therefore we can establish a correspondence between symmetry breaking and disorder in 2×2 RPE.

Appendix D. Comparison of fidelity between $N = 2$ and large N

In case of GOE, the analytical expression of fidelity for $N \gg 1$ [87] is compared with $\langle R(t) \rangle_{N=2}$ in table D1. We observe that $\langle R(t) \rangle$ behaves in a qualitatively similar way for both $N = 2$ and $N \gg 1$ with the exception of an oscillation decaying as $\propto t^{-3}$ in the intermediate time for $N \gg 1$. Similarly for GUE, $\langle R(t) \rangle$ attains minimum at $t_{\text{Th}} = \sqrt{\frac{3}{2}} \approx 1.22474$ where $\langle R(t_{\text{Th}}) \rangle = \frac{2}{3} \left(1 - e^{-\frac{3}{2}}\right) \approx 0.517913$. On the other hand, $t_{\text{R}} \approx 3.0196$ for $\epsilon = 10^{-3}$ using large- t expansion of $\langle R(t) \rangle$. Corresponding relative depth of correlation hole is $\kappa \equiv 1 - \frac{\langle R(t_{\text{Th}}) \rangle}{\bar{R}} = e^{-\frac{3}{2}} \approx 0.22313$.

Appendix E. Change of variables for 2×2 S-RPE

Normalized eigenvectors of a symplectic matrix have the form

$$|\Psi\rangle = \frac{1}{2\sqrt{2\csc^2\zeta - 1}} \begin{pmatrix} -\cot\frac{\zeta}{2}(\sin\alpha\cos\theta + i\cos\alpha\sin\phi) \\ -\cot\frac{\zeta}{2}(-\cos\alpha\cos\phi + i\sin\alpha\sin\theta) \\ \tan\frac{\zeta}{2}(\sin\alpha\cos\theta + i\cos\alpha\sin\phi) \\ \tan\frac{\zeta}{2}(-\cos\alpha\cos\phi + i\sin\alpha\sin\theta) \end{pmatrix} \quad (\text{E.1})$$

Then we can use the change of variables in table E1 with Jacobian of transformation, $|J| = \frac{1}{32}(E_1 - E_2)^4 |\sin^3\zeta \sin 2\alpha|$. Then for 2×2 S-RPE, the density in matrix space

u	v	x
$\frac{(E_1+E_2)+(E_1-E_2)\cos\zeta}{2}$	$\frac{(E_1+E_2)-(E_1-E_2)\cos\zeta}{2}$	$\frac{E_1-E_2}{2} \sin\zeta \cos\alpha \cos\phi$
y	z	w
$\frac{E_1-E_2}{2} \sin\zeta \cos\alpha \sin\phi$	$\frac{E_1-E_2}{2} \sin\zeta \sin\alpha \cos\theta$	$\frac{E_1-E_2}{2} \sin\zeta \sin\alpha \sin\theta$

Table E1. Change of variables for 2×2 symplectic matrix.

can be written as

$$\begin{aligned} P(H) &= \frac{1}{8\pi^3\sigma^4} \exp\left(-\frac{u^2+v^2}{2} - \frac{x^2+y^2+z^2+w^2}{2\sigma^2}\right) \\ \Rightarrow P(\vec{E}, \zeta, \alpha, \theta, \phi) &= \frac{1}{2^8\pi^3\sigma^4} |\sin^3 \zeta \sin 2\alpha| (E_1 - E_2)^4 e^{-\frac{E_1^2+E_2^2}{2} + \frac{(E_1-E_2)^2}{4} \sin^2 \zeta (1-\frac{1}{2\sigma^2})} \end{aligned} \quad (\text{E.2})$$

where $\sigma^2 = \frac{1}{2^{\gamma+1}}$. Note that ζ here plays the role of 2θ in case of O and U-RPE.

- [1] M.V. Berry and M. Tabor. Level clustering in the regular spectrum. *Proceedings of the Royal Society of London A: Mathematical, Physical and Engineering Sciences*, 356(1686):375–394, 1977.
- [2] Freeman J. Dyson. The threefold way. algebraic structure of symmetry groups and ensembles in quantum mechanics. *Journal of Mathematical Physics*, 3(6):1199–1215, 1962.
- [3] Alexander Altland and Martin R. Zirnbauer. Nonstandard symmetry classes in mesoscopic normal-superconducting hybrid structures. *Phys. Rev. B*, 55:1142–1161, Jan 1997.
- [4] O. Bohigas, M. J. Giannoni, and C. Schmit. Characterization of chaotic quantum spectra and universality of level fluctuation laws. *Phys. Rev. Lett.*, 52:1–4, Jan 1984.
- [5] Michael Victor Berry. Semiclassical theory of spectral rigidity. *Proceedings of the Royal Society of London. A. Mathematical and Physical Sciences*, 400(1819):229–251, 1985.
- [6] M V Berry. Regular and irregular semiclassical wavefunctions. *Journal of Physics A: Mathematical and General*, 10(12):2083–2091, dec 1977.
- [7] Thomas Gorin, Tomaž Prosen, Thomas H. Seligman, and Marko Žnidarič. Dynamics of loschmidt echoes and fidelity decay. *Physics Reports*, 435(2):33–156, 2006.
- [8] Eduardo Jonathan Torres-Herrera, Jonathan Karp, Marco Távora, and Lea F Santos. Realistic many-body quantum systems vs. full random matrices: Static and dynamical properties. *Entropy*, 18(10):359, 2016.
- [9] Eduardo Jonathan Torres-Herrera and Lea F. Santos. Dynamical detection of level repulsion in the one-particle aubry-andré model. *Condensed Matter*, 5(1), 2020.
- [10] Michael Schreiber, Sean S. Hodgman, Pranjal Bordia, Henrik P. Lüschen, Mark H. Fischer, Ronen Vosk, Ehud Altman, Ulrich Schneider, and Immanuel Bloch. Observation of many-body localization of interacting fermions in a quasirandom optical lattice. *Science*, 349(6250):842–845, 2015.
- [11] Jagannath Sutradhar, Subroto Mukerjee, Rahul Pandit, and Sumilan Banerjee. Transport, multifractality, and the breakdown of single-parameter scaling at the localization transition in quasiperiodic systems. *Phys. Rev. B*, 99:224204, Jun 2019.
- [12] Arijit Halder, Prosenjit Halder, Surajit Bera, Ipsita Mandal, and Sumilan Banerjee. Quench, thermalization, and residual entropy across a non-fermi liquid to fermi liquid transition. *Phys. Rev. Res.*, 2:013307, Mar 2020.
- [13] Wei-Bin Ni and Wen-Jia Rao. Describing the level statistics along many-body localization transition by short-range plasma model. *Physics Letters A*, 420:127747, 2021.
- [14] Wen-Jia Rao. Critical level statistics at the many-body localization transition region. *Journal of Physics A: Mathematical and Theoretical*, 54(10):105001, feb 2021.
- [15] T Prosen and M Robnik. Energy level statistics and localization in sparsed banded random matrix ensemble. *Journal of Physics A: Mathematical and General*, 26(5):1105–1114, mar 1993.
- [16] Jagannath Sutradhar, Soumi Ghosh, Sthitadhi Roy, David E. Logan, Subroto Mukerjee, and Sumilan Banerjee. Scaling of the fock-space propagator and multifractality across the many-body localization transition. *Phys. Rev. B*, 106:054203, Aug 2022.
- [17] Nilanjan Roy, Jagannath Sutradhar, and Sumilan Banerjee. Diagnostics of nonergodic extended states and many body localization proximity effect through real-space and fock-space excitations. *Physical Review B*, 107(11):115155, 2023.
- [18] C. E. Porter, editor. *Statistical theories of spectra: fluctuations*. Academic Press, 1965.
- [19] Manuel Pino, Lev B Ioffe, and Boris L Altshuler. Nonergodic metallic and insulating phases of josephson junction chains. *Proceedings of the National Academy of Sciences*, 113(3):536–541, 2016.
- [20] M. Pino, V. E. Kravtsov, B. L. Altshuler, and L. B. Ioffe. Multifractal metal in a disordered josephson junctions array. *Phys. Rev. B*, 96:214205, Dec 2017.
- [21] A. De Luca, B. L. Altshuler, V. E. Kravtsov, and A. Scardicchio. Anderson localization on the bethe lattice: Nonergodicity of extended states. *Phys. Rev. Lett.*, 113:046806, Jul 2014.
- [22] I. García-Mata, O. Giraud, B. Georgeot, J. Martin, R. Dubertrand, and G. Lemarié. Scaling

- theory of the anderson transition in random graphs: Ergodicity and universality. *Phys. Rev. Lett.*, 118:166801, Apr 2017.
- [23] S. Ray, A. Ghosh, and S. Sinha. Drive-induced delocalization in the aubry-andré model. *Phys. Rev. E*, 97:010101, Jan 2018.
 - [24] Yucheng Wang, Long Zhang, Wei Sun, Ting-Fung Jeffrey Poon, and Xiong-Jun Liu. Quantum phase with coexisting localized, extended, and critical zones. *Phys. Rev. B*, 106:L140203, Oct 2022.
 - [25] Sibaram Ruidas and Sumilan Banerjee. Many-body chaos and anomalous diffusion across thermal phase transitions in two dimensions. *SciPost Phys.*, 11:087, 2021.
 - [26] Norbert Rosenzweig and Charles E. Porter. Repulsion of energy levels in complex atomic spectra. *Phys. Rev.*, 120:1698–1714, Dec 1960.
 - [27] Akhilesh Pandey. Brownian-motion model of discrete spectra. *Chaos, Solitons & Fractals*, 5(7):1275 – 1285, 1995. Quantum Chaos: Present and Future.
 - [28] Akhilesh Pandey. Statistical properties of many-particle spectra. iv. new ensembles by stieltjes transform methods. *Annals of Physics*, 134(1):110–127, 1981.
 - [29] Pragya Shukla. Level statistics of anderson model of disordered systems: connection to brownian ensembles. *Journal of Physics: Condensed Matter*, 17(10):1653, feb 2005.
 - [30] Pierre Mergny and Satya N Majumdar. Stability of large complex systems with heterogeneous relaxation dynamics. *Journal of Statistical Mechanics: Theory and Experiment*, 2021(12):123301, 2021.
 - [31] Marco Biroli, Hernan Larralde, Satya N. Majumdar, and Grégory Schehr. Extreme statistics and spacing distribution in a brownian gas correlated by resetting. *Phys. Rev. Lett.*, 130:207101, May 2023.
 - [32] J. X. de Carvalho, M. S. Hussein, M. P. Pato, and A. J. Sargeant. Symmetry-breaking study with deformed ensembles. *Phys. Rev. E*, 76:066212, Dec 2007.
 - [33] J. X. de Carvalho, Sarika Jalan, and M. S. Hussein. Deformed gaussian-orthogonal-ensemble description of small-world networks. *Phys. Rev. E*, 79:056222, May 2009.
 - [34] Adway Kumar Das and Anandamohan Ghosh. Chaos due to symmetry-breaking in deformed poisson ensemble. *Journal of Statistical Mechanics: Theory and Experiment*, 2022(6):063101, 2022.
 - [35] Adway Kumar Das and Anandamohan Ghosh. Transport in deformed centrosymmetric networks. *Phys. Rev. E*, 106:064112, Dec 2022.
 - [36] V E Kravtsov, I M Khaymovich, E Cuevas, and M Amini. A random matrix model with localization and ergodic transitions. *New Journal of Physics*, 17(12):122002, dec 2015.
 - [37] M Pino, J Tabanera, and P Serna. From ergodic to non-ergodic chaos in rosenzweig–porter model. *Journal of Physics A: Mathematical and Theoretical*, 52(47):475101, oct 2019.
 - [38] Per von Soosten and Simone Warzel. Non-ergodic delocalization in the rosenzweig–porter model. *Letters in Mathematical Physics*, 109(4):905–922, 2019.
 - [39] Cécile Monthus. Multifractality of eigenstates in the delocalized non-ergodic phase of some random matrix models: Wigner–weisskopf approach. *Journal of Physics A: Mathematical and Theoretical*, 50(29):295101, jun 2017.
 - [40] Xiaodong Zhang, Weihua Zhang, Jiongning Che, and Barbara Dietz. Experimental test of the rosenzweig–porter model for the transition from poisson to gaussian unitary ensemble statistics, 2023.
 - [41] Boris L. Altshuler, Yuval Gefen, Alex Kamenev, and Leonid S. Levitov. Quasiparticle lifetime in a finite system: A nonperturbative approach. *Phys. Rev. Lett.*, 78:2803–2806, Apr 1997.
 - [42] I. M. Khaymovich, V. E. Kravtsov, B. L. Altshuler, and L. B. Ioffe. Fragile extended phases in the log-normal rosenzweig–porter model. *Phys. Rev. Research*, 2:043346, Dec 2020.
 - [43] I. M. Khaymovich and V. E. Kravtsov. Dynamical phases in a “multifractal” Rosenzweig–Porter model. *SciPost Phys.*, 11:45, 2021.
 - [44] G. De Tomasi, M. Amini, S. Bera, I. M. Khaymovich, and V. E. Kravtsov. Survival probability

- in Generalized Rosenzweig-Porter random matrix ensemble. *SciPost Phys.*, 6:14, 2019.
- [45] E Bogomolny and M Sieber. Eigenfunction distribution for the rosenzweig-porter model. *Physical Review E*, 98(3):032139, 2018.
 - [46] M. Amini. Spread of wave packets in disordered hierarchical lattices. *EPL (Europhysics Letters)*, 117(3):30003, feb 2017.
 - [47] Davide Facchetti, Pierpaolo Vivo, and Giulio Biroli. From non-ergodic eigenvectors to local resolvent statistics and back: A random matrix perspective. *EPL (Europhysics Letters)*, 115(4):47003, aug 2016.
 - [48] Davide Venturelli, Leticia F Cugliandolo, Grégory Schehr, and Marco Tarzia. Replica approach to the generalized rosenzweig-porter model. *SciPost Physics*, 14(5):110, 2023.
 - [49] Georg Lenz and Fritz Haake. Reliability of small matrices for large spectra with nonuniversal fluctuations. *Phys. Rev. Lett.*, 67:1–4, Jul 1991.
 - [50] Jean-Louis Pichard and Boris Shapiro. A matrix ensemble with a preferential basis and its application to disordered metals and insulators. *Journal de Physique I*, 4(5):623–628, 1994.
 - [51] Jonas Larson and Themistoklis Mavrogordatos. *The Jaynes–Cummings Model and Its Descendants*. 2053-2563. IOP Publishing, 2021.
 - [52] Subhasish Dutta Gupta, Nirmalya Ghosh, and Ayan Banerjee. *Wave optics: Basic concepts and contemporary trends*. CRC Press, 2015.
 - [53] B. R. Mollow. Power spectrum of light scattered by two-level systems. *Phys. Rev.*, 188:1969–1975, Dec 1969.
 - [54] M. I. Makin, Jared H. Cole, Charles Tahan, Lloyd C. L. Hollenberg, and Andrew D. Greentree. Quantum phase transitions in photonic cavities with two-level systems. *Phys. Rev. A*, 77:053819, May 2008.
 - [55] MV Berry and S Klein. Transparent mirrors: rays, waves and localization. *European Journal of Physics*, 18(3):222, 1997.
 - [56] Ramy El-Ganainy, Konstantinos G Makris, Mercedeh Khajavikhan, Ziad H Musslimani, Stefan Rotter, and Demetrios N Christodoulides. Non-hermitian physics and pt symmetry. *Nature Physics*, 14(1):11–19, 2018.
 - [57] Carl M Bender, MV Berry, and Aikaterini Mandilara. Generalized pt symmetry and real spectra. *Journal of Physics A: Mathematical and General*, 35(31):L467, 2002.
 - [58] F Caycedo-Soler, A Mattioni, J Lim, T Renger, SF Huelga, and Martin B Plenio. Exact simulation of pigment-protein complexes unveils vibronic renormalization of electronic parameters in ultrafast spectroscopy. *Nature Communications*, 13(1):2912, 2022.
 - [59] A. M. Zagorin, S. Ashhab, J. R. Johansson, and Franco Nori. Quantum two-level systems in josephson junctions as naturally formed qubits. *Phys. Rev. Lett.*, 97:077001, Aug 2006.
 - [60] Falk Töppel, Marco Ornigotti, and Andrea Aiello. Goos–hänchen and imbert–fedorov shifts from a quantum-mechanical perspective. *New Journal of Physics*, 15(11):113059, 2013.
 - [61] Jörg B. Götte, Wolfgang Löffler, and Mark R. Dennis. Eigenpolarizations for giant transverse optical beam shifts. *Phys. Rev. Lett.*, 112:233901, Jun 2014.
 - [62] Niladri Modak, Swain Ashutosh, Shyamal Guchhait, Sayantan Das, Alok Kumar Pan, and Nirmalya Ghosh. Longitudinal and transverse optical beam shifts show non-separability. *Laser & Photonics Reviews*, n/a(n/a):2300166.
 - [63] Ioana Dumitriu and Alan Edelman. Matrix models for beta ensembles. *Journal of Mathematical Physics*, 43(11):5830–5847, 2002.
 - [64] M.L. Mehta. *Random Matrices*. Pure and Applied Mathematics. Elsevier Science, 2004.
 - [65] V. K. B. Kota and S. Sumedha. Transition curves for the variance of the nearest neighbor spacing distribution for poisson to gaussian orthogonal and unitary ensemble transitions. *Phys. Rev. E*, 60:3405–3408, Sep 1999.
 - [66] P Chau Huu-Tai, N A Smirnova, and P Van Isacker. Generalized wigner surmise for (2×2) random matrices. *Journal of Physics A: Mathematical and General*, 35(15):L199, 2002.
 - [67] M V Berry and P Shukla. Spacing distributions for real symmetric 2×2 generalized gaussian

- ensembles. *Journal of Physics A: Mathematical and Theoretical*, 42(48):485102, 2009.
- [68] TA Brody. A statistical measure for the repulsion of energy levels. *Lettere al Nuovo Cimento (1971-1985)*, 7(12):482–484, 1973.
 - [69] M V Berry and M Robnik. Semiclassical level spacings when regular and chaotic orbits coexist. *Journal of Physics A: Mathematical and General*, 17(12):2413, 1984.
 - [70] F.M. Izrailev. Quantum localization and statistics of quasienergy spectrum in a classically chaotic system. *Physics Letters A*, 134(1):13 – 18, 1988.
 - [71] S. Sorathia, F. M. Izrailev, V. G. Zelevinsky, and G. L. Celardo. From closed to open one-dimensional anderson model: Transport versus spectral statistics. *Phys. Rev. E*, 86:011142, Jul 2012.
 - [72] Roberto Merlin. Rabi oscillations, floquet states, fermi’s golden rule, and all that: Insights from an exactly solvable two-level model. *American Journal of Physics*, 89(1):26–34, 2021.
 - [73] Adway Kumar Das and Anandamohan Ghosh. Eigenvalue statistics for generalized symmetric and hermitian matrices. *Journal of Physics A: Mathematical and Theoretical*, 52(39):395001, sep 2019.
 - [74] Fritz Haake. *Introduction*, pages 1–14. Springer Berlin Heidelberg, Berlin, Heidelberg, 2010.
 - [75] Mauro Schiulaz, E. Jonathan Torres-Herrera, and Lea F. Santos. Thouless and relaxation time scales in many-body quantum systems. *Phys. Rev. B*, 99:174313, May 2019.
 - [76] Peter Forrester. Beta ensembles. In *The Oxford Handbook of Random Matrix Theory*. Oxford University Press, 2011.
 - [77] Ricardo Marino, Satya N Majumdar, Gregory Schehr, and Pierpaolo Vivo. Number statistics for β -ensembles of random matrices: applications to trapped fermions at zero temperature. *Physical Review E*, 94(3):032115, 2016.
 - [78] Pierpaolo Vivo and Satya N. Majumdar. On invariant 2×2 β -ensembles of random matrices. *Physica A: Statistical Mechanics and its Applications*, 387(19):4839–4855, 2008.
 - [79] Romain Allez, Jean-Philippe Bouchaud, Satya N Majumdar, and Pierpaolo Vivo. Invariant β -wishart ensembles, crossover densities and asymptotic corrections to the marčenko–pastur law. *Journal of Physics A: Mathematical and Theoretical*, 46(1):015001, 2012.
 - [80] Fabio Deelan Cunden, Francesco Mezzadri, and Pierpaolo Vivo. A unified fluctuation formula for one-cut β -ensembles of random matrices. *Journal of Physics A: Mathematical and Theoretical*, 48(31):315204, 2015.
 - [81] Adway Kumar Das and Anandamohan Ghosh. Nonergodic extended states in the β ensemble. *Phys. Rev. E*, 105:054121, May 2022.
 - [82] Adway Kumar Das, Anandamohan Ghosh, and Ivan M. Khaymovich. Absence of mobility edge in short-range uncorrelated disordered model: Coexistence of localized and extended states, 2023.
 - [83] Freeman J. Dyson. Statistical theory of the energy levels of complex systems. i. *Journal of Mathematical Physics*, 3(1):140–156, 1962.
 - [84] G. Le Caër, C. Male, and R. Delannay. Nearest-neighbour spacing distributions of the β -hermite ensemble of random matrices. *Physica A: Statistical Mechanics and its Applications*, 383(2):190–208, 2007.
 - [85] Apollonas S. Matsoukas-Roubeas, Mathieu Beau, Lea F. Santos, and Adolfo del Campo. A self-averaging spectral form factor implies unitarity breaking, 2023.
 - [86] E. J. Torres-Herrera and Lea F. Santos. Dynamical manifestations of quantum chaos: correlation hole and bulge. *Philosophical Transactions of the Royal Society A: Mathematical, Physical and Engineering Sciences*, 375(2108):20160434, 2017.
 - [87] E. J. Torres-Herrera, Antonio M. García-García, and Lea F. Santos. Generic dynamical features of quenched interacting quantum systems: Survival probability, density imbalance, and out-of-time-ordered correlator. *Phys. Rev. B*, 97:060303, Feb 2018.
 - [88] Matthias Christandl, Nilanjana Datta, Artur Ekert, and Andrew J Landahl. Perfect state transfer in quantum spin networks. *Physical review letters*, 92(18):187902, 2004.
 - [89] Matthias Christandl, Nilanjana Datta, Tony C Dorlas, Artur Ekert, Alastair Kay, and Andrew J

- Landahl. Perfect transfer of arbitrary states in quantum spin networks. *Physical Review A*, 71(3):032312, 2005.
- [90] Thomas Guhr, Axel Müller-Groeling, and Hans A. Weidenmüller. Random-matrix theories in quantum physics: common concepts. *Physics Reports*, 299(4):189 – 425, 1998.
- [91] W.-H. Steeb and A. J. van Tonder. Quantum mechanics and a completely integrable dynamical system. *Zeitschrift für Naturforschung A*, 42(8):819–824, 1987.
- [92] F Haake and G Lenz. Classical hamiltonian dynamics of rescaled quantum levels. *Europhysics Letters*, 13(7):577, 1990.